Role of Hexahistidine in Directed Nanoassemblies of Tobacco Mosaic Virus Coat Protein

Michael A. Bruckman,[†,§] Carissa M. Soto,[†,§] Heather McDowell,[†] Jinny L. Liu,[†] Banahalli R. Ratna,[†,*] Katalin V. Korpany,[‡] Omar K. Zahr,[‡] and Amy Szuchmacher Blum[‡,*]

[†]Center for Bio/Molecular Science and Engineering, Naval Research Laboratory, 4555 Overlook Avenue SW, Washington, D.C. 20375, United States and [‡]Department of Chemistry, McGill University, 801 Sherbrooke Street West, Montreal, QC, H3A 2K6, Canada. [§] These authors contributed equally to this work.

ABSTRACT A common challenge in nanotechnology is the fabrication of materials with well-defined nanoscale structure and properties. Here we report that a genetically engineered tobacco mosaic virus (TMV) coat protein (CP), to which a hexahistidine (His) tag was incorporated, can self-assemble into disks, hexagonally packed arrays of disks, stacked disks, helical rods, fibers, and elongated rafts. The insertion of a His tag to the C-terminus of TMV-CP was shown to significantly affect the self-assembly in comparison to the wild type, WT-TMV-CP. Furthermore, the His tag interactions attributed to the alternative self-assembly of His-TMV-CP can be controlled through ethanol and nickel-nitrilotriacetic acid (Ni-NTA) additions as monitored with atomic force microscopy.

KEYWORDS: tobacco mosaic virus · atomic force microscopy · self-assembly · transmission electron microscopy · His-tagged protein · *Escherichia coli*

Major breakthroughs in nanotechnology, such as molecular sensors and magnetic nanoparticle-based data storage devices, require breakthroughs in the precise positioning of individual components with subnanometer resolution.[1] Because "top-down" manipulation of materials on this length scale is problematic, researchers have set out to develop methods by which different components in solution can come together in an ordered fashion.[2] This self-assembly process is very efficient provided the components are properly encoded to do so.[3,4] Biological scaffolds present an innovative means to organize materials on the nanoscale with precise control over position and degree of saturation, due to the specificity of biological interactions.[5−7] Use of plant viruses as nanosized scaffolds for devices offers the promise of exquisite control for positioning on the nanoscale.[8] Furthermore, virus templates can both undergo further self-assembly into extended structures and template the simultaneous creation of many identical complex submicrometer geometrical structures. In recent years, tobacco mosaic virus (TMV) has proved useful in assembling materials for many applications such as nanoscale electronics[9−12] energy storage,[13] and light harvesting.[14]

TMV is an RNA virus that infects plants, especially tobacco and its relatives.[15,16] The wild type (WT) virus consists of 17 copies of a single coat protein assembled into 18 nm disks;[17] 129 copies of these disks stack around the TMV RNA genome to form a tube that is 300 nm long and 18 nm in diameter.[18] TMV tubes have recently been used as a template for materials such as inorganic nanoparticles[13,19−21] and the conducting polymer, polyaniline.[9−12] In the absence of the TMV genome, TMV coat protein (WT-TMV-CP) can be isolated as three major assembled components: protein A (a dynamic equilibrium between monomers, trimers, and pentamers of WT-TMV-CP),[22] disks consisting of 34 monomers (also known as the 20S structure), and helical rods of various lengths.[17] WT-TMV-CP assemblies in solution can be controlled to favor protein A, disks, or rods depending on the pH and ionic strength.[22] Furthermore, the dominant species of WT-TMV-CP in solution is also dependent on temperature. For example, at pH 5.0 in 20 mM sodium acetate, the WT-TMV-CP exists predominantly as protein A at 4 °C and as rods at room temperature. This behavior has been shown to be fully reversible—a room temperature solution of rods at pH 5.0 will disassemble into a solution of protein A when stored at 4 °C.[23,24] Previous work involving modification of the WT-TMV-CP either through genetic engineering[14,25,26] or chemical modifications[27−31] did not significantly

* Address correspondence to ratna@nrl.navy.mil, amy.blum@mcgill.ca.

Received for review April 13, 2010 and accepted January 27, 2011.

Published online February 25, 2011
10.1021/nn1025719

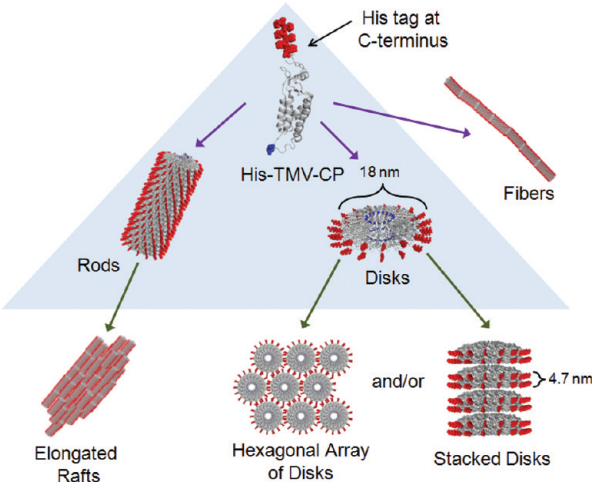

Scheme 1. Self-assembling structures of His-TMV-CP. Incorporated His tag shown in red. Amino acid E97 is highlighted in blue for 3D perception. Transitions in the highlighted region also occur for WT-TMV-CP. Transitions outside the highlighted area occur for His-TMV-CP over time, with the rate of formation dependent on solution pH and ionic strength. Model crystal structure of His-TMV-CP generated from modulating the crystal structure of WT-TMV-CP using PyMol (www.pymol.org) with coordinates obtained from RCSB Protein Data Bank (www.pdb.org). PDB ID: 1EI7 and 2TMV for the disk and helical rod structures, respectively.

change the equilibrium conditions between the various assemblies.

Although WT-TMV-CP has been available as a recombinant protein expressed in *Escherichia coli* for many years,[32,33] to date no one has reported the addition of a His tag to WT-TMV-CP. Typically the His tag is introduced into proteins to facilitate their purification.[34,35] The His tag chelates to Ni^{2+} contained on commercially available nickel-nitrilotriacetic acid (Ni-NTA) packing materials.[36] This allows purification of recombinant proteins in a single step, often without affecting the biological activity of engineered proteins. In an attempt to maintain the physical properties (*i.e.*, self-assembly of disks and rods) of WT-TMV-CP, the His tag was incorporated at the C-terminus. According to the crystal structure of WT-TMV-CP,[37] the C-terminus is solvent accessible and not involved in the major intramolecular interactions responsible for protein folding. Furthermore, the C-terminus is located at the exterior of the WT-TMV-CP disks (Scheme 1). Thus, we anticipated that the modified protein should fold properly and self-assemble following behavior described in the equilibrium phase map presented by Klug.[22]

Here, we present data on the behavior of TMV-CP containing a His tag inserted at the C-terminus of the protein (His-TMV-CP) and compare its properties to WT-TMV-CP. We demonstrate that the His tag provides an additional handle in which self-assembly could be tuned by modulating the interactions introduced by the His tag. One of the potential issues with using WT-TMV-CP as a scaffold is that the assembled structures (rods, disks) exist in equilibrium with monomeric and oligomeric forms (protein A), and that this equilibrium limits the useable range of solution conditions for additional modifications. The presence of the His tag on our construct greatly enhances the suitability of His-TMV-CP as a scaffold for nanoscale structures. The addition of six histidine residues to each CP monomer extends the equilibrium phase with a disk majority into higher and lower pH conditions when compared to the WT. In addition, the core assembled components formed from His-TMV-CP (protein A, disks, and helical rods) can undergo additional hierarchical assembly into extended structures such as fibers, hexagonally closed packed islands, and elongated rafts depending on the solution conditions, as shown in Scheme 1. The stability of all self-assembled structures is greatly enhanced *versus* WT-TMV-CP as a result of interactions between the His tags. Furthermore, the His tag allows chemical control of the majority structure independent of the solution pH and ionic strength, which greatly extends the usable solution conditions for His-TMV-CP as a template.

RESULTS AND DISCUSSION

Production of His-TMV-CP. Successful construction of His-TMV-CP expression plasmids was performed. As shown in Figure 1A, lane 1, the PCR product corresponding to the insert which encodes for the His-TMV-CP, migrated as expected at 500 bp position compared to DNA marker (lane M). Corresponding clones were sent for sequencing, and the correct sequence was obtained. The sequence alignment is included in the Supporting Information (Figure 1S). DNA sequence of His-TMV-CP is identical to the WT-TMV-CP except the presence of C-terminal $(His)_6$ in His-TMV-CP DNA. The sequence confirmed clone, His-TMV-CP-2, was successfully subcloned to the expression host, Rosetta2(DE3)-pLysS for protein expression. Expression was tested at first in a small scale experiment in which the final volume was 25 mL. Once protein production was confirmed by SDS-PAGE of whole cell lysates, 500 mL expressions were carried out and the target protein

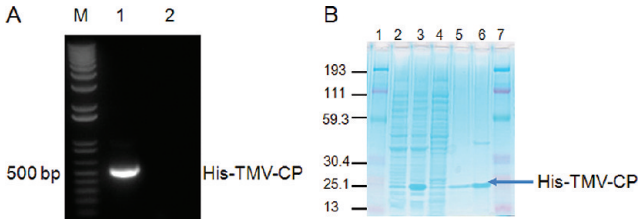

Figure 1. Generation of His-TMV-CP DNA fragments, expression, and purification of target protein. (A) 1% agarose gel of His-TMV-CP fragments. As shown in lane 1, amplified PCR product ran at 500 bp position compared to DNA marker (lane M). Lane 2 is a negative control without DNA template. (B) SDS-PAGE of His-TMV-CP expression and purification. Protein molecular weight standards are shown in lanes 1 and 7. Numbers on the left are the MW of the standards in kDa. Lanes 2 and 3 are from 1 mL aliquots of whole cell lysates from 500 mL culture. Lane 2 shows the uninduced control (t = 0) and lane 3 corresponds to the culture after expression (t = final). A new protein band in lane 3 at position 18.5 kDa corresponds to the target protein His-TMV-CP (blue arrow). Lane 4 is the soluble fraction of cell pellet after lysis. Purified protein is shown in lanes 5 and 6.

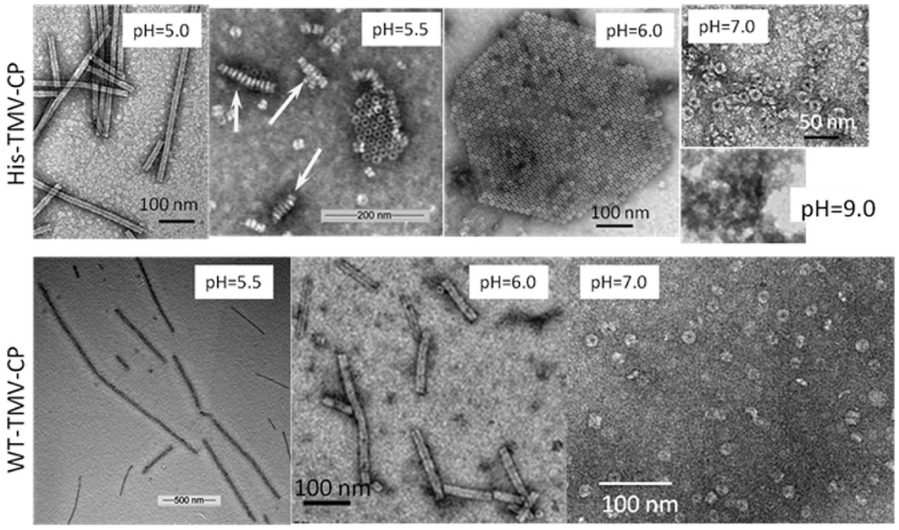

Figure 2. His-TMV-CP and WT-TMV-CP samples in 400 mM buffer after 4 days at 4 °C at various pHs. As pH increases, the dominant structure changes from rods to disks. This transition occurs at a lower pH for His-TMV-CP (pH 5.5) than for WT-TMV-CP (pH 7.0). His-TMV-CP shows some additional extended structures. At pH 5.5, there are some stacked disks (indicated by white arrows) and some small hexagonally packed islands. At pH 6.0, hexagonally packed islands are the dominant structure and are much larger in size. At pH 9.0, both TMV-CP proteins are in protein A form (Supporting Information, Figure 3S).

purified. As shown in Figure 1B, target protein was produced in the induced cells, shown as an intense new protein band in lane 3. The protein ran between protein standards 25.1 and 13 kDa (orange and pink bands) as expected since the calculated molecular weight of the target protein is 18.5 kDa. As shown in lanes 5 and 6 of Figure 1B, protein purification was accomplished since the major band is at the expected position for the target protein. It is important to note that the faint band at higher position (>30.4 kDa) in lane 6 corresponds to the dimer of the target protein. The dimer can be dissociated by adding 100 mM KOH in a 4:1 ratio of KOH to protein (v/v) followed by incubation at room temperature (RT) for 30 min prior to the addition of corresponding volume of 2× sample buffer for SDS-PAGE. Such treatment promoted the dimer to break apart which resulted in a single band in SDS-PAGE in comparison to nontreated sample (see Supporting Information, Figure 2S). A total of 10 mg of purified protein were recovered from a 500 mL culture as quantified by the Bradford assay.

Assembly of His-TMV-CP: Protein A to Disks and Rods. As described in Materials and Methods, protein refolding and further self-assembly was carried out at protein concentration of 1.7 mg/mL. It was found that the concentration of His-TMV-CP was quite important. At protein concentrations above 2 mg/mL, the protein precipitates. Resulting aggregates do not show any of the polymorphic structures typically known for WT-TMV-CP. Conversely, at protein concentrations below 0.5 mg/mL, at all pH values and ionic strengths tested, protein assemblies lacked any kind of organization when imaged by TEM. Throughout the text no distinctions are made between sodium and potassium phosphate buffers; they are simply referred as phosphate buffer since both gave similar results in the assembly of His-TMV-CP.

Initial experiments in self-assembly of His-TMV-CP were focused on the conditions known to produce disks and rods in the WT-TMV-CP.[30] Briefly, coat protein is denatured in 100 mM KOH followed by dialysis in 10 mM or 100 mM phosphate buffer at pH 8.5 to have

the protein in the protein A form. Indeed TEM data indicates that the protein assemblies at pH 8.5 lack any particular structure (Supporting Information, Figure 3S-A) and only structures with heights smaller than the expected for the disks (2 nm) were found (Figures 3S-B, 3S-D). Samples are dialyzed from pH 8.5 to corresponding pH values of 8.0, 7.0, or 6.0. His-TMV-CP samples at pH 8.0 show the presence of the disks, which is not observed for the WT-TMV-CP control, which remains as protein A. Disks were observed for the His-TMV-CP over the entire pH range of 8.0−6.0 at buffer concentrations of 100 and 10 mM (Figures 6S and 7S) and at buffer concentrations of 400 mM (Figure 2), which is a broader area in comparison to the WT-TMV-CP control where the disks are typically observed at pH 6.5−7.0 at comparable ionic strengths (Figure 2).

As buffer concentration increases, and surface charge is better screened, the interactions between neighboring TMV disks increase, leading to structures in His-TMV-CP that are not seen for WT-TMV-CP under similar conditions, such as stacked disks (indicated by arrows in Figure 2, pH 5.5) and hexagonally packed islands (Figure 2, pH 5.5 and 6.0). The stacked disks consist of interacting sets of 20-S disk structures, unlike the helical rods, which are continuous chiral structures that show no internal seams and a clearly visible central pore. The hexagonally packed islands tend to form slowly even at low ionic strength, but the rate of assembly is greatly increased as buffer concentration increases. At 400 mM, these extended structures become the dominant species in solution after 24 h incubation time (Figure 2, pH 6.0).

The extended assembled structure is pH dependent. At pH 6.0, hexagonally packed disks are observed as the dominant structure. However as the pH drops, the disks are also assembled into stacked disks, as can clearly be observed in Figure 2, pH 5.5. Although stacked disks are observed with WT-TMV-CP, these structures are typically observed at pH above 7.0 and high (>600 mM) ionic strength. The hexagonally packed disks are a novel assembly for His-TMV-CP—there is no analog in WT-TMV-CP under any solution conditions reported to date, since WT-TMV-CP disks without His tags pack in a rectangular lattice (reported from TEM observations).[38] It is important to note that we ascertained that the self-assembly is not occurring *in-situ* on the grid during the drying process. Extended hexagonally-packed disks were observed only in samples left to undergo the self-assembly process at least for a period of 24 h. There was no evidence of hexagonal self-assembly when the samples were analyzed as soon as the sample was prepared and after 6 h. When the sample was imaged at zero incubation time, only protein A was observed. At the 6 h incubation period, even though disks were seen, no extended assembly was present. On the basis of these observations and given the fact that the sample for TEM imaging is generally prepared by drying a small drop (20 μl) of the solution on the grid for only 2 min we believe the self-assembly to be occurring in solution. We are currently exploring different chemistries to utilize the highly ordered arrays of disks for the realization of inorganic−organic hybrid materials for novel photonic applications.

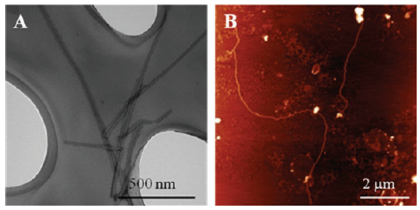

Figure 3. His-TMV-CP long fiber formation. The presence of the His tag greatly enhances assembly stability, enabling the formation of very long fibers (>2 μm) not seen for WT-TMV-CP under similar conditions. (A) TEM image of sample incubated at room temperature (400 mM and pH 5.5) for 24 h where rods are the dominant species for WT-TMV-CP. (B) AFM image of sample incubated at 4 °C (25 mM boric acid and pH 8.3) for 4 days where disks or monomer should be the dominant species for WT-TMV-CP.

For further assembly of the disks into rods, His-TMV-CP samples in 100 mM phosphate buffer at pH 8.5 were dialyzed against 100 mM sodium acetate buffer pH 5.5. TEM images show the presence of short rods (<300 nm) at those conditions (Supporting Information, Figure 6S, pH 5.5) and longer rods (>300 nm) at pH 5.0 (Figure 6S, pH 5.0) which are also the predominant forms for the WT-TMV-CP but at slightly different conditions. For the WT-TMV-CP at 100 mM buffer concentration long rods are observed at pH 5.5 while short rods are seen at pH 6.0 (Figures 4S and 6S). Furthermore, for the His-TMV-CP disks are found at 100 mM buffer concentration, pH 6.0 (Figure 6S, pH 6.0) conditions in which the WT-TMV-CP is predominantly in the rod assembly. This confirms that indeed even at lower ionic strength at pH 6.0 for the His-TMV-CP, the disk assembly is the predominant specie (Figure 7S).

Enhanced Stability and Fiber Formation from Protein A. In early experiments, a macroscopic precipitation was observed for His-TMV-CP (pH 8.0; 1 mg/mL: 100 mM phosphate, 16 h dialysis) at room temperature. Optical microscopy revealed extended fiberlike structures (data not shown). Such aggregation is not observed for the WT-TMV-CP, where protein A is the predominant species at pH 8.0 and 100 mM phosphate. At pH 5.5 after 24 h incubation at RT, His-TMV-CP assembly resulted in long fibers (Figure 3A). To further understand this assembly process, we observed similar solutions at 4 °C instead of room temperature to slow down the assembly process. Allowing 4 days of incubation in 25 mM boric acid at pH 8.3 and 4 °C, the dominant structure of His-TMV-CP is extended fibers that remain soluble. Figure 3B shows AFM images of such fibers after two weeks incubation at 4 °C. These

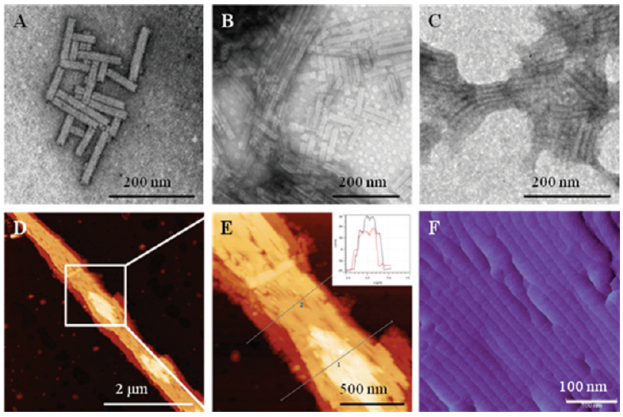

Figure 4. Elongated raft formation from assembled rods. At buffer concentration 100 mM and pH 5.5, His-TMV-CP assembles to rods initially. Over time, formation of elongated rafts is observed. Elongated rafts, as defined herein, are composed of multiple His-TMV-CP rods arranged side-by-side. TEM images clearly show (A) the formation of rods initially followed by (B) a mixture of isolated rods and rafts. Finally, (C) rafts are the only structure observed. (D) The elongated rafts can extend over 15 μm, as seen with atomic force microscopy (AFM). (E) Upon closer inspection (corresponding section inside white square in panel D), rods can be clearly distinguished in the elongated rafts and layers of rods can also be seen (with height image). Inset shows cross sections through the narrow axis. Step heights are 15 nm. (F) Amplitude image (magnified from panel E) shows that the elongated rafts consist of assembled rods. The resulting assembly is from refolded His-TMV-CP after 6 days of incubation at 4 °C at pH 5.25 (D−F).

fiber assemblies extended over a length of 5−10 μm and were consistently around 15 nm in height. The length of individual fibers is much longer than observed for WT-TMV-CP.[17] This is likely due to the additional stabilization provided by the His tag interactions, which reduces the frequency of long helices breaking into shorter ones. In addition, these extended fibers were found to be stable at pH values >6 that would otherwise be represented by disk structures or protein A with WT-TMV-CP.[17]

Equilibrium trapping of extended fibers at low temperature or high pH requires stabilization of the rod assemblies that constitute a minor phase of the equilibrium mixture. This can be accomplished by stabilizing the interactions between assembling units such that the rate of disassembly is much slower than the rate of assembly. For His-TMV-CP, the introduction of the aromatic histidine groups could result in enhanced interactions that overcome the electrostatic repulsions present between neighboring CP groups. The effect of introducing aromatic moieties on TMV assembly[39] and the His-Tag in peptides that support fibrillar structures[40] has been previously examined. Briefly, the chemical incorporation of pyrene into TMV coat protein resulted in extended rod assemblies to lengths 6−8 times longer than native TMV rods at pH 5.5 and continued to stabilize rod structures at pH 7.6, where disks are expected to be the predominant species. This enhanced stability was due to π-stacking between the pyrene moieties.[39] This is qualitatively similar to the observed structures of His-TMV-CP, which extend over micrometers and show a greatly enhanced range not just for stability but also for assembly.

Temperature Dependence of Disks and Rods Assembly. The temperature dependence of self-assembly in solutions of WT-TMV-CP and His-TMV-CP was compared, since this is directly related to the structure stability. Solutions of both WT-TMV-CP and His-TMV-CP at 2 mg/mL, 25 mM potassium phosphate at pH 5.63 were incubated for 24 h at room temperature, and AFM samples were prepared. The solutions were then returned to 4 °C, incubated for 24 h, and prepared as AFM samples. As expected, rod assemblies formed in both samples at room temperature. The WT-TMV-CP samples consisted of discrete rods, as has been previously reported.[22] For the His-TMV-CP sample at room temperature, rod assemblies were also observed. However, the rods were generally incorporated into large disordered aggregations, which were not seen in the WT-TMV-CP samples. When the samples were returned to 4 °C, the WT-TMV-CP rods disassembled into protein A. Since WT-TMV-CP assembly is an entropically driven, endothermic process, disassembly of the rods at low temperatures is expected.[23] However, the His-TMV-CP samples not only remained assembled at 4 °C, but continued to agglomerate into insoluble aggregations that ultimately crashed out of solution (data not shown). Unlike in the case of WT-TMV-CP, rod formation of His-TMV-CP at room temperature is no longer a reversible process. Thus, His-TMV-CP shows enhanced stability of the rod assemblies as compared to rod assemblies of WT-TMV-CP since the His-TMV-CP rods stay intact in response to an stimulus, unlike the WT-TMV-CP rods that go back to Protein A. To avoid agglomeration during long-term storage and determine conditions to stabilize rods and disks over extended periods of time, a series of studies were performed in which several chemical additives were added to the protein solution (Supporting Information, Table 1S). Ni-NTA and ethanol were the most successful additives to control the rods and disks assemblies. Those results are discussed in detail in the following section.

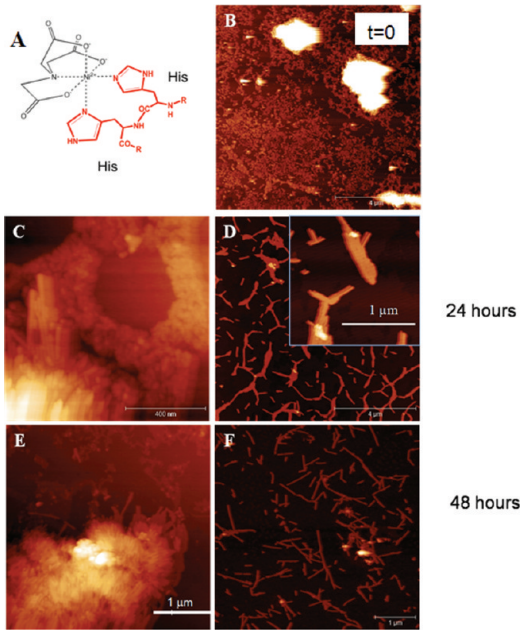

Figure 5. Disassembly of His-TMV-CP elongated rafts by the addition of Ni-NTA. (A) Schematic showing complex formation between two histidines (red) and Ni-NTA. (B) AFM image at time *t* = 0 showing freshly folded His-TMV-CP. (C) AFM image of control sample (His-TMV-CP without Ni-NTA) at *t* = 24 h. Note formation of elongated rafts in bottom left corner. (D) AFM image of Ni-NTA containing sample at time *t* = 24 h showing dispersed rods and bundles of rods. No large aggregates were found. Inset shows details of "broken rafts" structures. (E) AFM image of control sample (His-TMV-CP without Ni-NTA) at *t* = 48 h. Image shows large rafts structures (>1 μm). (F) AFM image of Ni-NTA containing sample at time *t* = 48 h showing isolated rods.

Hierarchical Assembly into Extended Structures and Chemical Control of Assembly. *Elongated Rafts Formation from Assembled Rods.* His-TMV-CP forms extended assemblies at all pH and ionic strengths tested if the solution is incubated long enough. Figure 4 shows TEM and AFM images of structures composed of helical rods. Figure 4D illustrates a typical AFM image taken of the refolded His-TMV-CP after 6 days of incubation at 4 °C at pH 5.25. Figure 4D reveals an assembled His-TMV-CP raft composed of elongated His-TMV-CP rods assembled side by side. These raft assemblies have been seen to extend upward of 15 μm in length with a cross section of 0.5−1.0 μm. Rafts heights are variable along the length of the assembly, but tend to be in multiples of approximately 15 nm (Figure 4E), which is slightly smaller than the diameter of assembled WT-TMV-CP rods. As well, the constituent elongated His-TMV-CP rod widths vary between 15 and 20 nm, and therefore correspond well to the expected rod diameter of 18 nm seen for the native virus.

We attribute the observed stabilization of the rod assemblies (elongated rafts) in His-TMV-CP to interactions between His tags of adjacent subunits. The presence of significant amounts of EDTA (25 mM) into the His-TMV-CP solution is expected to chelate any divalent cations that would otherwise contribute to structural stabilization *via* salt bridges.[41] In separate experiments, the addition of EDTA (25 mM) into the protein solution did not perturb the assembly of elongated rafts (data not shown). Furthermore, "irreversible" assembly of His-TMV-CP into elongated rafts can be reversed by the

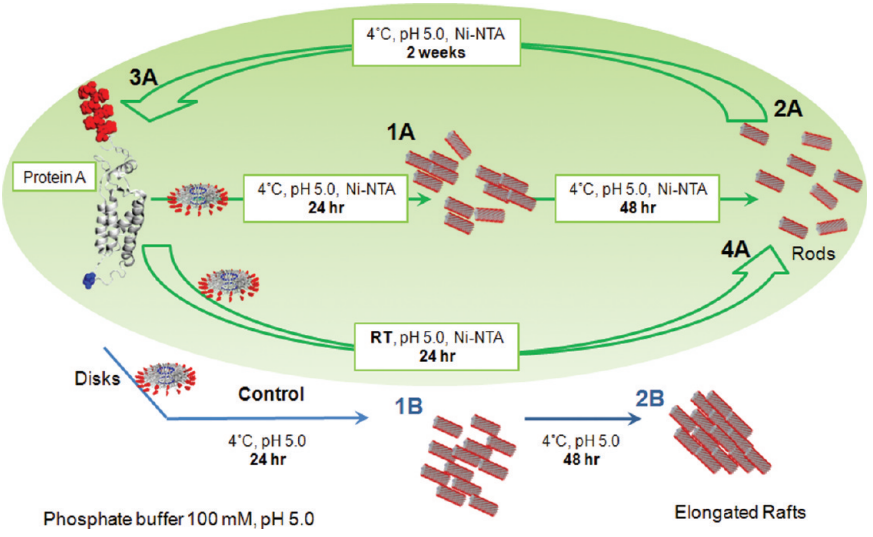

Scheme 2. Schematic representation of the interaction of Ni-NTA with His-TMV-CP at different time points in the experiment (pathway inside green oval). His-TMV-CP protein A on the left, where the His-tag is depicted in red, assembles into disks, rods, and elongated rafts depending on reaction conditions. At first both Ni-NTA (1A) and non-containing Ni-NTA control (1B) assemble into rods that arrange side by side into small domains. After 48 h at 4°C, the Ni-NTA containing samples dissociate into individual rods (2A) while the negative control (no Ni-NTA) self-assemble further into the elongated rafts (2B). After 2 weeks incubation at 4°C the Ni-NTA containing sample goes back to Protein A (3A). Lastly, His-TMV-CP in the protein A form in the presence of Ni-NTA at room temperature (RT) is able to self-assemble into individual rods (4A).

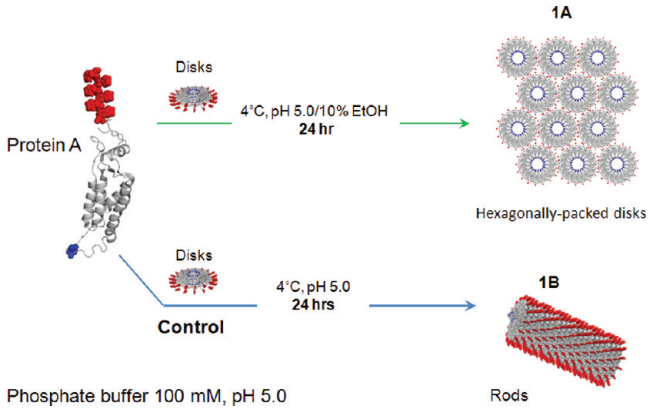

Scheme 3. Schematic representation of the effect that ethanol addition to a final concentration of 10% has on His-TMV-CP at 100 mM phosphate pH 5.0. After a 24 h incubation in the presence of 10% ethanol, the pre-assembled disks self-assemble into a hexagonally close-packed structure (1A), while the negative control lacking any ethanol assembled into rods (1B).

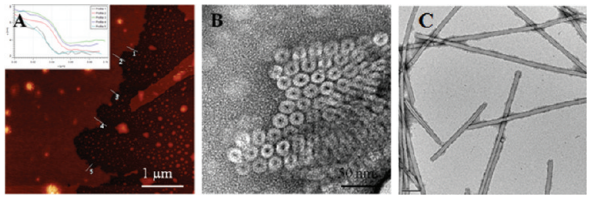

Figure 6. TMV-CP in 100 mM phosphate pH 5.0, 10% ethanol after incubation at 4 °C for 24 h. (A) AFM topography of extended island consisting of hexagonally packed disks of His-TMV-CP. Inset shows linear cross sections with uniform step height of 3.8 ± 0.5 nm. (B) TEM image of the same sample showing hexagonal packing. (C) TEM of WT-TMV-CP control experiment showing rod formation in 100 mM phosphate pH 5.5, 10% ethanol.

addition of Ni-NTA to the solution. The Ni-NTA is expected to coordinate with the histidines,[36] (Figure 5A) to break the interactions between the His tags on neighboring TMV assembled rods.

To study this phenomenon, 10 mM Ni-NTA was added to 2 mg/mL freshly folded His-TMV-CP in 25 mM phosphate, pH 5.0, as shown in Scheme 2. After incubation at 4 °C for 24 h, AFM images showed a mixture of broken up elongated rafts structures and isolated rod assemblies (Figure 5D). After incubation at 4 °C for 48 h, AFM images showed exclusively isolated rod assemblies (Figure 5F). Images taken after 2 weeks at 4 °C showed that the sample consisted predominately of protein A, which is the expected structure for WT-TMV-CP stored at 4 °C and pH 5.0.[23] This protein A material rapidly formed TMV rod assemblies when incubated at room temperature for 24 h (data not shown).

The sequence of images in Figure 5 suggests that the His-TMV-CP rapidly assembles into rods and bundles of rods which are assumed to be the precursor of the elongated raft structure, even at 4 °C. This assembly process involves interactions among His-tags on the neighboring rods. When the sample is exposed to Ni-NTA such large assemblies disassemble into smaller rod structures and 48 h after the initial introduction of Ni-NTA, the His−His interactions between neighboring rod structures have been replaced by interactions of His-tag with Ni-NTA, leading to isolated TMV rod assemblies (Figure 5F) that are not the predominant species in the negative control (Figure 5E). Over time the Ni-NTA continues to chelate the majority of the His tags on the His-TMV-CP, leading to the return of WT-TMV-CP-like behavior, as shown by the presence of the protein A form at 4 °C after 2 weeks. The interaction between the His tag and the Ni-NTA complex does not interfere with the assembly of the His-TMV-CP, as Ni-NTA conjugated His-TMV-CP in protein A form readily forms rods when returned to room temperature (Scheme 2, 4A). This protein A material saturated with Ni-NTA shows qualitatively the same behavior as WT-TMV-CP with regard to assembly, stability, and temperature. The reversibility of the elongated rafts assembly process by usage of Ni-NTA brings the possibility in which by precisely controlling the protein to Ni-NTA ratio one can control the size of the assemblies and ultimately the applicability of such materials.

Hexagonally Packed Island Formation from Disks. To control the assembly of His-TMV-CP into rods and disks, buffer additives were used to control the interactions between subunits. The effect of the His tag was "turned off" through the addition of 10 mM Ni-NTA, as described above to keep the rods from agglomeration. In contrast, exposing the His-TMV-CP to ethanol (Scheme 3) prevented rod formation entirely at the tested temperatures, even at pH 5.0 where rods should be the predominant species in solution (Figure 6). The mechanism of disk stabilization is likely the suppression of "Caspar pair" formation due to changes in the conformation of the His

tag in the presence of ethanol. Caspar pairs consist of two carboxylates that can hydrogen bond, which reduces the electrostatic repulsion between subunits and are thought to stabilize the chiral helical disk structure which can assemble into rods.[23] If Caspar pair formation is suppressed, the dominant species in solution will be nonhelical disks, which are not thought to assemble further in solutions of WT-TMV-CP. In contrast, WT-TMV-CP assembles into rods even in the presence of 10% ethanol (Figure 6C). This indicates that the His tag is crucial in suppressing rod formation and therefore provides a handle for more precise control of the self-assembled structures formed by WT-TMV-CP. Further investigation into the mechanism of rod suppression *via* ethanol is currently underway.

Owing to the presence of the six histidines, if coat protein solutions containing ethanol are incubated at 4 °C, pH 5.0, the nonhelical disks arrange into hexagonal arrays when observed under AFM and TEM (Figure 6). These arrays extend over several micrometers with an approximate height of 3.8 ± 0.5 nm, which correlates well with the known height of ~4 nm for stacked disks. The root mean square (rms) roughness calculated from AFM images of these islands is 0.30 nm, which strongly suggests that these islands are constructed of a monolayer of individual nonhelical disks undergoing side-by-side organization. This is consistent with an interaction between His tags as the polypeptides are located around the circumference of the His-TMV-CP disks. In contrast to the observed rectangular lattice structure for WT-TMV-CP disks,[42,38] the His-TMV-CP island structure is hexagonally close-packed.

A His tag was successfully engineered to C-terminus of the tobacco mosaic virus coat protein. The presence of the His tag did not impede formation of assembled TMV structures such as rods and disks that had been previously observed in experiments with wildtype TMV coat protein. The stability zone of the disk assembly was greatly enhanced by the incorporation of His tag in TMV coat protein when compared to the majority disk region of stability for WT-TMV-CP. Furthermore, the His tag greatly enhanced the stability of assembled rod structures, rendering this assembly irreversible with respect to temperature, in contrast to the WT coat protein. In addition to the extended zone of stability for the disk structure found in His-TMV-CP, it is also possible to eliminate rod formation altogether in His-TMV-CP *via* the addition of ethanol to a final concentration of 10% to the solution.

The attachment of the His tag creates an additional chemical handle for the control of the structures formed by His-TMV-CP, enabling new forms of hierarchical assembly and extending the range of solution conditions suitable for TMV scaffolded nanostructures. All three major protein assemblies (protein A, disks, and rods) can organize into extended hierarchical structures that are not seen for WT-TMV-CP due to interparticle interactions induced by the presence of the His tag. Once the His-TMV coat protein assembles into the disks or rods seen for WT-TMV-CP, these assembled entities can themselves act as subunits, producing larger structures through interactions between neighboring histidine tags. These interactions can be tuned through the addition of Ni-NTA to the solution, which complexes to the His tag, and prevents interactions between neighboring His tags. The addition of ethanol prevents further assembly into rod structures for His-TMV-CP, even under solution conditions favorable for rod formation for WT-TMV-CP. Further studies are underway to examine the dependence of the assembly process on the concentration of Ni-NTA in solution. The addition of a chemical control on assembly, makes His-TMV-CP an even more versatile scaffold for the assembly of nanostructured materials.

MATERIALS AND METHODS

Materials were from USA sources and used as received. Enzymes NdeI, NcoI, and T4 DNA ligase were purchased from New England BioLabs Inc. (Ipswich, MA). XL1 Blue *E. coli* strain was from Stratagene, Agilent Technology (La Jolla, CA). pET20b vector, *E. coli* Rosetta2(DE3)pLysS, Lysonase, and Bug Buster reagent were from EMD Biosciences, Inc. (Madison, WI). Ampicillin, chloramphenicol, β-mercaptoethanol, potassium/sodium phosphate salts, potassium chloride (KCl), EDTA, nickel(II)nitrate hexahydrate, nitrilotriacetic acid trisodium salt, potassium hydroxide (KOH), RNase A (EC 3.1.25.5), and phenylmethane sulfonyl fluoride (PMSF; protease inhibitor) were purchased from Sigma-Aldrich (St. Louis, MO). Luria Broth (LB) media was purchased from Invitrogen (Carlsbad, CA). Isopropyl-1-thio-β-D-galactoside (IPTG) was obtained from G-Biosciences (St. Louis, MO). Precasted 4−20% precise protein gels (SDS-PAGE), Gel Code stain reagent, dialysis cassettes, and Slide-A-Lyzer MINI dialysis units were obtained from Pierce (Rockford, IL). DNase I (from bovine pancreas grade II) was purchased from Roche Diagnostics (Indianapolis, IN). Ni-NTA Superflow was purchased from QIAGEN (Valencia, CA). Ethanol 200 proof was acquired from The Warner-Graham Co. (Cockeysville, MD). Imidazole was purchased from Fisher Scientific Co. (Pittsburgh, PA). All buffers and media were prepared in Milli-Q water (18 MΩ). Buffers were filter sterilized using 0.2 μm filters (Nalgene, Fisher Scientific Pittsburgh, PA). Uranyl acetate was from SPI Supplies (West Chester, PA) and 300-mesh Formvar-carbon-coated copper grids for TEM were from Electron Microscopy Sciences (Hatfield, PA). The Quick Start Bradford Protein Assay (protein concentration determination) and Kaleidodscope prestained broad range protein standards (for SDS-PAGE) were purchased from Bio-Rad Laboratories, Inc. (Hercules, CA). DNA sequencing was performed by the Biopolymer Laboratory at University of Maryland at Baltimore.

Construction of His-TMV-CP Expression Plasmids. pTMVP,[14] a wild type TMV cDNA clone, was a kind gift from M. B. Francis, from the University of California, Berkley. Two primers, TMVCP F1, GATTCGTTTTACATATGTCTTACAGTATCACTAC[13] and His-TMV-CP R1, TAGTACCATGGTCATTAGTGATGGTGATGGTGATGAGTTGCAGGACCAGAGGTC, were used to amplify TMV coat protein (WT-TMV-CP), gp6 from pTMVCP templates. Conditions for

amplification were 35 cycles of 95 °C for 30 s, 55 °C for 30 s, and 68 °C for 30 s. The resulting amplified fragments were then digested with NdeI and NcoI and were subsequently inserted into pET20b vectors DNA using T4 DNA ligase. The ligation mixture was then electroporated into XL1 Blue and plated on LB plates supplemented with 100 μg/mL of ampicillin for overnight incubation at 37 °C. Plasmid DNA was then isolated from three potential positive clones grown on the plates and were sent out for DNA sequencing. The sequence confirmed clones, His-TMV-CP-2, containing 6× His at C-terminus was then subcloned to the expression host, Rosetta2(DE3)pLysS for protein expression.

His-TMV-CP Expression and Purification. In general, *E. coli* Rosetta2(DE3)pLysS containing the desired expression plasmid was grown in LB media supplemented with 100 μg/mL ampicillin and 25 μg/mL chloramphenicol at 30 °C with constant shaking at 250 rpm. Detailed procedure: a single colony from an agar plate (streaked from frozen glycerol stocks and grown for 24 h at 30 °C) was used for inoculation of a 5 mL media; cells were grown for 16 h until saturation. A 1 mL portion of the saturated culture was used to inoculate 25 mL of media and this mixture was allowed to grow until OD at 600 nm ($OD_{600\ nm}$) reached 0.50−0.60. Cells were used for inoculation of 500 mL of media and grown at 30 °C until $OD_{600\ nm}$ 0.50−0.60. Prior to induction, cells were incubated for 5 min at 25 °C and a 1 mL aliquot was kept for further analysis ($t = 0$), after which IPTG was added to a final concentration of 10 μM. The induced culture was shaken overnight at 25 °C, 250 rpm. A 1 mL aliquot was kept for expression assessment (t = final) prior to harvesting. Cells were harvested by centrifugation at 17600g (Sorval RC-6 plus) for 10 min at 15 °C. The recovered pellet (wt cells: 5 g) was resuspended in 15 mL of lysis buffer (50 mM potassium phosphate (KP), 300 mM KCl, pH 8.0) and kept frozen at −80 C for further purification of the target protein.

Evaluation of the expression was performed by analysis of whole cell lysates in SDS-PAGE. Cell pellets from 1 mL aliquots were resuspended in 50 mM KP buffer pH 8.0 and frozen at −20 °C. Upon thawing 2× SDS-PAGE sample buffer was added, and samples were boiled for 5 min. Each well contained a final 0.2 $OD_{600\ nm}$.

The resuspended pellet from a 500 mL culture was thawed at RT followed by immediate addition of 1.5 mL of Bug Buster reagent, 30 μL of Lysonase, PMSF up to 1 mM, 5 μL of RNase A (10 mg/mL), and 5 μL of DNase I (10 mg/mL). The mixture was shaken at 250 rpm at 30 °C for 30 min. A 30 mL portion of cold equilibrating buffer (50 mM KP, 300 mM KCl, 1 mM PMSF, 10 mM β-mercaptoethanol, 10 mM imidazole, 10% ethanol; pH 8.0) was added, mixed, and incubated in ice for 5 min. The mixture was centrifuged at 11950g (Sorval RC-6 plus) for 20 min at 4 °C. The soluble fraction was mixed with 3 mL of Ni-NTA already in equilibrating buffer. The mixture was stirred overnight at 4 °C after which it was poured into a column, first at free flow until the flow stopped. For the rest of the purification the column was eluted by means of a peristaltic pump at 0.5 mL/min. The packing material was washed with 50 mL of cold wash buffer-20 (50 mM KP, 300 mM KCl, 1 mM PMSF, 10 mM β-mercaptoethanol, 20 mM imidazole, 10% ethanol; pH 8.0) and 50 mL of cold wash buffer-40 (50 mM KP, 300 mM KCl, 1 mM PMSF, 10 mM β-mercaptoethanol, 40 mM imidazole, 10% ethanol; pH 8.0). The target protein was eluted with cold elution buffer (50 mM KP, 300 mM KCl, 1 mM PMSF, 10 mM β-mercaptoethanol, 500 mM imidazole, 10% ethanol; pH 8.0). Elutions from the Ni-NTA column were frozen and kept at −20 °C until further use.

Protein concentration was determined by the Bradford method with just a minor change. For Bradford assay: 5 μL of corresponding protein elution was mixed with 5 μL of urea buffer (8 M urea, 100 mM KP buffer, 10 mM Tris, pH 7.4) and incubated at RT for 5 min to ensure proper solubilization of the protein. After solubilization 490 μL of PBS (50 mM KP, 150 mM NaCl, pH 7.2) were added, and the sample was vortexed; 150 μL of the protein solution was used for the Bradford assay. The same amount of urea buffer was added to the controls (γ-globulin) previously diluted in 495 μL of PBS for calibration curve preparation. Samples along with controls were assayed in duplicate.

Assembly of His-TMV-CP Disks and Rods. Control experiments for self-assembly were carried out in parallel using WT-TMV-CP from the WT-TMV native rods (see Supporting Information for details). His-TMV-CP solution was prepared by refolding as previously described for the WT-TMV-CP[30] with minor changes. His-TMV-CP stock solution at 1.0 mg/mL was centrifuged for 15 min at 4 °C at 9300g (Eppendorf Centrifuge 5415R). The pellet was recovered and dissolved in minimal 100 mM KOH added in 20 μL increments. The suspended pellet was incubated at 4 °C for 2 h. Protein concentration was determined by using absorbance values of the peak at 278 nm and previously reported extinction coefficient (ε = 1.3 mL mg^{-1} cm^{-1}).[43] A Varian Cary 5000 UV−vis−near-IR spectrometer (with Cary Win UV Scan Application version 3.00 software) was used for UV−visible measurements. Prior to dialysis, the concentration of His-TMV-CP was set to 1.7 mg/mL. The resulting solution was dialyzed against 10 or 100 mM potassium/sodium phosphate at pH 8.5 at 4 °C in a Slide-A-Lyzer MINI dialysis unit (10 kDa MWCO). At this stage the protein is refolded into the protein A form. Protein samples at pH 8.5 are dialyzed for 24 h at 4 °C against buffers at pH values 8.0, 7.0, or 6.0 at the desired ionic strength. For the assembly of rods a protein solution in 10/100 mM phosphate buffer pH 8.5 is dialyzed against 10 or 100 mM sodium acetate buffer, pH 5.5. For higher ionic strengths studies protein in 100 mM phosphate buffer pH 8.5 is dialyzed for 24 h at 4 °C against 400 mM phosphate buffer at pH values 8.0, 7.0, 6.0, or 400 mM sodium acetate pH 5.5.

His-TMV-CP Solutions for Temperature Dependence Studies and Hierarchical Assembly into Extended Structures. His-TMV-CP solution was prepared by refolding as previously described for the WT-TMV-CP[30] with minor changes. His-TMV-CP stock solution at 2 mg/mL was diluted to 2 mL in 100 mM KP buffer, pH 7.5, and centrifuged in a Sorvall RC6 plus with SH-3000 rotor (4700 rpm) at 4 °C for 2 h. Pellet was recovered and dissolved in 1 mL of 100 mM KOH added in 20 μL increments. The suspended pellet was incubated at 4 °C for two hours. Resulting solution was dialyzed against 10 mM KP pH 7.96, 25 mM in EDTA at 4 °C in a dialysis cassette (3.5 kDa MWCO). At this stage the protein is refolded into the protein A form. After 24 h, the dialysis buffer was changed to 100 mM KP pH 5.5, 25 mM in EDTA, and continued for another 24 h at 4 °C to promote self-assembly into rods. The concentration of the solution was determined by UV−visible spectroscopy at 278 nm (Hitachi U-2800) to be 1.7 mg/mL (ε = 1.3 mL mg^{-1} cm^{-1}).[43]

Reminder of stock His-TMV-CP (2 mg/mL) was supplemented with glycerol to a final concentration of 10%, flash frozen using liquid nitrogen, and stored at −20 °C until use.

Modulation of His-tag on His-TMV-CP Self-Assembled Structures. His-TMV-CP (1.7 mg/mL) previously assembled into rods was incubated in 100 mM KP, pH 5.0 containing ethanol (10% v/v) or 10 mM Ni-NTA complex (protein assembly solution lacked EDTA to avoid chelation of the Ni^{2+} and complications in the interpretation of the results). The Ni−NTA complex was prepared by mixing a 9:8 volume ratio of 0.1 M nickel(II)nitrate hexahydrate and 0.1 M nitrilotriacetic acid trisodium salt in 100 mM KP, pH 5.0, and heated at 55 °C for 15 min. The concentration of the free complex was determined by UV−visible spectroscopy at 625 nm (ε = 5.5 M^{-1} cm^{-1}).[44]

AFM Imaging of Extended Fibers and Elongated Rafts. A 10 μL portion of each sample was deposited on freshly cleaved mica (muscovite mica, grade V-4, SPI) incubated at RT for 5 min, rinsed with 5 mL of distilled water, and dried in air. AFM images of extended fibers were obtained of the solutions upon first exposure, after 24 h, and after 48 h. Solutions were kept at 4 °C throughout the study. For imaging the elongated rafts, after 6 days at 4 °C, pH 5.25, 20 μL of the aliquoted refolded His-TMV-CP was deposited onto freshly cleaved mica. Protein was incubated for 20 min, after which excess protein solution was wicked off and the sample left to air-dry. The sample was then washed by immersion in distilled water for 1 min, wicked dry, and then dried in air.

Tapping mode AFM experiments were carried out using the Digital Instruments Multimode SPM (Veeco, Santa Barbara, US) with standard etched silicon probes (Nanoworld, Neuchatel, CH) having a typical spring constant of 42 N/m. Solutions were

kept at 4 °C throughout. Image analysis was carried out using Gwyddion version 2.18.

TEM Imaging. A 20 μL portion of protein solution was deposited onto a 300-mesh Formvar-carbon-coated copper grid for 2 min. The grid was then stained with 20 μL of 2% uranyl acetate and characterized with a LIBRA-120 EFTEM.

Acknowledgment. We thank M. Francis for the expression plasmid pTMVP-WT and Q. Wang for wild-type native TMV. A. S. Blum gratefully acknowledges the support of the Natural Sciences and Engineering Research Council of Canada. B. Ratna thanks the Office of Naval Research for financial support and M. Bruckman and H. McDowell for postdoctoral fellowships from the National Research Council. C.M. Soto thanks M. Archer for technical assistance with AFM. We thank A. Adams and C. Spillmann for reviewing the manuscript.

Supporting Information Available: Detailed DNA sequencing data of His-TMV-CP expression plasmid; AFM data of His-TMV-CP assembled into protein A; TEM and AFM data of control experiments on the self-assembly of WT-TMV-CP into disks and rods; methods for recovery of WT-TMV-CP from native WT-TMV; TEM data from self-assembly experiments of His-TMV-CP and WT-TMV-CP samples in 100 mM buffer at various pH values. This material is available free of charge *via* the Internet at http://pubs.acs.org.

REFERENCES AND NOTES

1. Bishop, K. J. M.; Wilmer, C. E.; Soh, S.; Grzybowski, B. A. Nanoscale Forces and Their Uses in Self-Assembly. *Small* **2009,** *5*, 1600–1630.
2. Lu, W.; Lieber, C. M. Nanoelectronics from the Bottom Up. *Nat. Mater.* **2007,** *6*, 841–850.
3. Whitesides, G. M.; Grzybowski, B. Self-Assembly at All Scales. *Science* **2002,** *295*, 2418–2421.
4. Ismagilov, R. F.; Schwartz, A.; Bowden, N.; Whitesides, G. M. Autonomous Movement and Self-Assembly. *Angew. Chem., Int. Ed.* **2002,** *41*, 652–654.
5. Seeman, N. C.; Belcher, A. M. Emulating Biology: Building Nanostructures from the Bottom Up. *Proc. Natl. Acad. Sci. U.S.A.* **2002,** *99*, 6451–6455.
6. Young, M.; Willits, D.; Uchida, M.; Douglas, T. Plant Viruses as Biotemplates for Materials and Their Use in Nanotechnology. *Annu. Rev. Phytopathol.* **2008,** *46*, 361–384.
7. Fan, T. X.; Chow, S. K.; Zhang, D. Biomorphic Mineralization: From Biology to Materials. *Prog. Mater. Sci.* **2009,** *54*, 542–659.
8. Singh, P.; Gonzalez, M. J.; Manchester, M. Viruses and Their Uses in Nanotechnology. *Drug Dev. Res.* **2006,** *67*, 23–41.
9. Niu, Z.; Liu, J.; Lee, L. A.; Bruckman, M.; Zhao, D.; Koley, G.; Wang, Q. Biological Templated Synthesis of Water-Soluble Conductive Polymeric Nanowires. *Nano Lett.* **2007,** *7*, 3729–3733.
10. Niu, Z.; Bruckman, M. A.; Li, S.; Lee, L. A.; Lee, B.; Pingali, S. V.; Thiyagarajan, P.; Wang, Q. Assembly of Tobacco Mosaic Virus into Fibrous and Macroscopic Bundled Arrays by Aniline Polymerization on Its Surface. *Langmuir* **2007,** *23*, 6719–6724.
11. Niu, Z. W.; Bruckman, M.; Kotakadi, V. S.; He, J. B.; Emrick, T.; Russell, T. P.; Yang, L.; Wang, Q. Study and Characterization of Tobacco Mosaic Virus Head-to-Tail Assembly Assisted by Aniline Polymerization. *Chem. Commun.* **2006,** 3019–3021.
12. Bruckman, M. A.; Niu, Z.; Li, S.; Lee, L. A.; Varazo, K.; Nelson, T. L.; Lavigne, J. J.; Wang, Q. Development of Nanobiocomposite Fibers by Controlled-Assembly of Rod-like Tobacco Mosaic Virus. *Nanobiotechnology* **2007,** *3*, 31–39.
13. Royston, E.; Ghosh, A.; Kofinas, P.; Harris, M. T.; Culver, J. N. Self-Assembly of Virus-Structured High Surface Area Nanomaterials and Their Application as Battery Electrodes. *Langmuir* **2008,** *24*, 906–912.
14. Miller, R. A.; Presley, A. D.; Francis, M. B. Self-Sssembling Light-Harvesting Systems from Synthetically Modified Tobacco Mosaic Virus Coat Proteins. *J. Am. Chem. Soc.* **2007,** *129*, 3104–3109.
15. Harrison, B. D.; Wilson, T. M. Milestones in the Research on Tobacco Mosaic Virus. *Philos. Trans. R. Soc. London, B* **1999,** *354*, 521–529.
16. Culver, J. N. Tobacco Mosaic Virus Assembly and Disassembly: Determinants in Pathogenicity and Resistance. *Annu. Rev. Phytopathol.* **2002,** *40*, 287–308.
17. Butler, J. G. The Current Picture of the Structure and Assembly of Tobacco Mosaic Virus. *J. Gen. Virol.* **1984,** *65*, 253–279.
18. Lomonossoff, G. P.; Butler, P. J. Assembly of Tobacco Mosaic Virus: Elongation towards the 3′-Hydroxyl Terminus of the RNA. *FEBS Lett.* **1980,** *113*, 271–274.
19. Royston, E.; Brown, A. D.; Harris, M. T.; Culver, J. N. Preparation of Silica Stabilized Tobacco Mosaic Virus Templates for the Production of Metal and Layered Nanoparticles. *J. Colloid Interface Sci.* **2009,** *332*, 402–407.
20. Lee, S. Y.; Choi, J.; Royston, E.; Janes, D. B.; Culver, J. N.; Harris, M. T. Deposition of Platinum Clusters on Surface-Modified Tobacco Mosaic Virus. *J. Nanosci. Nanotechnol.* **2006,** *6*, 974–981.
21. Dujardin, E.; Peet, C.; Stubbs, G.; Culver, J. N.; Mann, S. Organization of Metallic Nanoparticles Using Tobacco Mosaic Virus Templates. *Nano Lett.* **2003,** *3*, 413–417.
22. Klug, A. The Tobacco Mosaic Virus Particle: Structure and Assembly. *Philos. Trans. R. Soc. London, B* **1999,** *354*, 531–535.
23. Kegel, W. K.; van Der Schoot, P. Physical Regulation of the Self-Assembly of Tobacco Mosaic Virus Coat Protein. *Biophys. J.* **2006,** *91*, 1501–1512.
24. Sturtevant, J. M.; Velicelebi, G.; Jaenicke, R.; Lauffer, M. A. Scanning Calorimetric Investigation of the Polymerization of the Coat Protein of Tobacco Mosaic Virus. *Biochemistry* **1981,** *20*, 3792–3800.
25. Culver, J. N.; Dawson, W. O.; Plonk, K.; Stubbs, G. Site-Directed Mutagenesis Confirms the Involvement of Carboxylate Groups in the Disassembly of Tobacco Mosaic Virus. *Virology* **1995,** *206*, 724–730.
26. Yi, H.; Nisar, S.; Lee, S. Y.; Powers, M. A.; Bentley, W. E.; Payne, G. F.; Ghodssi, R.; Rubloff, G. W.; Harris, M. T.; Culver, J. N. Patterned Assembly of Genetically Modified Viral Nanotemplates *via* Nucleic Acid Hybridization. *Nano Lett.* **2005,** *5*, 1931–1936.
27. Lee, L. A.; Wang, Q. Adaptations of Nanoscale Viruses and Other Protein Cages for Medical Applications. *Nanomedicine: NBM* **2006,** *2*, 137–149.
28. Lee, L. A.; Niu, Z. W.; Wang, Q. Viruses and Virus-like Protein Assemblies: Chemically Programmable Nanoscale Building Blocks. *Nano Res.* **2009,** *2*, 349–364.
29. Li, K.; Nguyen, H. G.; Lu, X. B.; Wang, Q. Viruses and Their Potential in Bioimaging and Biosensing Applications. *Analyst* **2010,** *135*, 21–27.
30. Schlick, T. L.; Ding, Z.; Kovacs, E. W.; Francis, M. B. Dual-Surface Modification of the Tobacco Mosaic Virus. *J. Am. Chem. Soc.* **2005,** *127*, 3718–3723.
31. Bruckman, M. A.; Kaur, G.; Lee, L. A.; Xie, F.; Sepulveda, J.; Breitenkamp, R.; Zhang, X.; Joralemon, M.; Russell, T. s. P.; Emrick, T.; Wang, Q. Surface Modification of Tobacco Mosaic Virus with "Click" Chemistry. *ChemBioChem* **2008,** *9*, 519–523.
32. Hwang, D. J.; Roberts, I. M.; Wilson, T. M. A. Expression of Tobacco Mosaic Virus Coat Protein and Assembly of Pseudovirus Particles in *Escherichia Coli*. *Proc. Natl. Acad. Sci. U.S.A.* **1994,** *91*, 9067–9071.
33. Shire, S. J.; McKay, P.; Leung, D. W.; Cachianes, G. J.; Jackson, E.; Woods, W. I.; Raghavendra, K.; Khairallah, L.; Schuster, T. M. Preparation and Properties of Recombinant DNA Derived Tobacco Mosaic Virus Coat Protein. *Biochemistry* **1990,** *29*, 5119–5126.
34. Porath, J.; Carlsson, J. A. N.; Olsson, I.; Belfrage, G. Metal Chelate Affinity Chromatography, A New Approach to Protein Fractionation. *Nature* **1975,** *258*, 598–599.
35. Hochuli, E.; Bannwarth, W.; Dobeli, H.; Gentz, R.; Stüber, D. Genetic Approach to Facilitate Purification of Recombinant Proteins with a Novel Metal Chelate Adsorbent. *Nat. Biotechnol.* **1988,** *6*, 1321–1325.
36. Hochuli, E.; Dobeli, H.; Schacher, A. New Metal Chelate Adsorbent Selective for Proteins and Peptides Containing

Neighboring Histidine Residues. *J. Chromatogr.* **1987,** *411*, 177–184.
37. Namba, K.; Pattanayek, R.; Stubbs, G. Visualization of Protein−Nucleic Acid Interactions in a Virus. Refined Structure of Intact Tobacco Mosaic Virus at 2.9 Å Resolution by X-ray Fiber Diffraction. *J. Mol. Biol.* **1989,** *208*, 307–325.
38. Dedeo, M. T.; Duderstadt, K. E.; Berger, J. M.; Francis, M. B. Nanoscale Protein Assemblies from a Circular Permutant of the Tobacco Mosaic Virus. *Nano Lett.* **2010,** *10*, 181–186.
39. Endo, M.; Wang, H.; Fujitsuka, M.; Majima, T. Pyrene-Stacked Nanostructures Constructed in the Recombinant Tobacco Mosaic Virus Rod Scaffold. *Chem.—Eur. J.* **2006,** *12*, 3735–3740.
40. Boothroyd, S.; Saiani, A.; Miller, A. F. Formation of Mixed Ionic Complementary Peptide Fibrils. *Macromol. Symp.* **2008,** *273*, 139–145.
41. Renzi, F.; Panetta, G.; Vallone, B.; Brunori, M.; Arceci, M.; Bozzoni, I.; Laneve, P.; Caffarelli, E. Large-Scale Purification and Crystallization of the Endoribonuclease XendoU: Troubleshooting with His-Tagged Proteins. *Acta Crystallogr.* **2006,** *F62*, 298–301.
42. Finch, J. T.; Gilbert, P. F. C.; Klug, A.; Leberman, R. X-ray Analysis of the Disk of Tobacco Mosaic Virus Protein: II. The Packing Arrangement in the Crystal. *J. Mol. Biol.* **1974,** *86*, 183–192.
43. Orlov, V. N.; Arutyunyan, A. M.; Kust, S. V.; Litmanovich, E. A.; Drachev, V. A.; Dobrov, E. N. Macroscopic Aggregation of Tobacco Mosaic Virus Coat Protein. *Biochemistry (Moscow)* **2001,** *66*, 154–162.
44. Laine, P.; Matilainen, R. Simultaneous Determination of DTPA, EDTA, and NTA by UV−Visible Spectrometry and HPLC. *Anal. Bioanal. Chem.* **2005,** *382*, 1601–1609.